

Molecular driving forces for water adsorption in MOF-808: A comparative analysis with UiO-66

Hilliary O. Frank^{1, a)} and Francesco Paesani^{1, 2, 3, 4, b)}

¹⁾*Department of Chemistry and Biochemistry, University of California San Diego, La Jolla, California 92093, United States*

²⁾*Materials Science and Engineering, University of California San Diego, La Jolla, California 92093, United States*

³⁾*Halicioğlu Data Science Institute, University of California San Diego, La Jolla, California 92093, United States*

⁴⁾*San Diego Supercomputer Center, University of California San Diego, La Jolla, California 92093, United States*

Metal-organic frameworks (MOFs), with their unique porous structures and versatile functionality, have emerged as promising materials for adsorption, separation, and storage of diverse molecular species. In this study, we investigate water adsorption in MOF-808, a prototypical MOF that shares the same secondary building unit (SBU) as UiO-66, and elucidate how differences in topology and connectivity between the two MOFs influence the adsorption mechanism. To this end, molecular dynamics (MD) simulations were performed to calculate several thermodynamic and dynamical properties of water in MOF-808 as a function of relative humidity (RH), from the initial adsorption step to full pore filling. At low RH, the μ_3 -OH groups of the SBUs form hydrogen bonds with the initial water molecules entering the pores, which triggers the filling of these pores before the μ_3 -OH groups in other pores become engaged in hydrogen bonding with water molecules. Our analyses indicate that the pores of MOF-808 become filled by water sequentially as the RH increases. A similar mechanism has been reported for water adsorption in UiO-66. Despite this similarity, our study highlights distinct thermodynamic properties and framework characteristics that influence the adsorption process differently in MOF-808 and UiO-66.

^{a)}Electronic mail: hfrank@ucsd.edu

^{b)}Electronic mail: fpaesani@ucsd.edu

I. INTRODUCTION

Water scarcity is a pressing global issue with far-reaching implications.¹⁻³ The emergence of water-insecure regions is intricately linked to rapid population growth, climate change, and water pollution.^{4,5} With projections indicating that two-thirds of the world’s population could face water shortages by 2025,⁶ devising solutions for clean water supply is critical. Currently, there are methods for water purification such as physical and chemical filtration, which include the treatment of seawater to produce drinkable water.⁷⁻⁹ However, these methods are associated with high costs and energy consumption, rendering them inaccessible to many communities.¹⁰ Another significant limitation is that these methods, primarily designed for treating seawater,^{11,12} are not suitable for landlocked regions.

Atmospheric water harvesting (AWH) represents a promising solution to the limitations inherent in current water purification methods.¹³ Since the air contains $\sim 10^{21}$ liters of water globally in the form of water vapor, AWH holds the potential to capture this water and supply it to water-scarce regions.¹⁴ In this context, metal-organic frameworks (MOFs), a class of porous materials constructed from inorganic secondary building units (SBUs) and organic linkers,¹⁵⁻¹⁸ have attracted significant interest as materials for AWH applications due to their large surface area and high tunability.¹⁸⁻²⁴

The assessment of MOFs for AWH applications is traditionally accomplished through experimental measurements of adsorption isotherms at varying temperatures and relative humidity (RH) values.^{20,21,25-28} However, the vast landscape of possible MOFs presents a formidable challenge, as it is impractical to experimentally assess the water adsorption capacity of every single framework. This scenario underscores the key role of computer simulations in identifying specific structural and physicochemical properties of MOFs that can lead to enhanced water adsorption capacity. Computational studies, therefore, not only augment our understanding of the adsorption mechanisms but can also guide in the design of MOFs optimized for AWH applications.^{18,29-34}

Understanding the behavior of water within MOFs through computer simulations presents several challenges, including the accurate description of water–framework and water–water interactions. Different computational approaches are currently available for modeling these interactions, ranging from empirical force fields (FFs) of various functional forms³⁵⁻⁴³ to ab initio methods based on wave function theory (WFT)⁴⁴ and density functional theory

(DFT).⁴⁵ Although correlated WFT methods, such as coupled cluster with single, double, and perturbative triple excitations, CCSD(T), the current “gold standard” for chemical accuracy, provide an accurate representation of molecular interactions^{46,47} without resorting to ad hoc simplifications, the associated computational cost is presently prohibitive for systems containing more than a handful of molecules. Despite recent progress in the development of efficient WFT methods, DFT remains the most common approach for ab initio simulations in periodic boundary conditions, such as those pertaining to the adsorption of water in MOFs.^{22,29,48–50} However, DFT suffers from inherent limitations due to the use of approximate exchange-correlation functionals and electron densities, which manifest in both functional-driven and density-driven errors^{51–57} that hinder the ability of current DFT models to accurately describe the properties of water.^{58–62} On the other hand, by adopting functional forms based on classical mechanics, common FFs exhibit limited accuracy and lack predictive power when modeling the properties of water across various thermodynamic conditions and in different environments.^{63–65}

Ten years ago, our group introduced MB-pol, a data-driven many-body potential for water rigorously derived from CCSD(T) data.^{66–68} MB-pol combines a physics-based model based on many-body electrostatics with data-driven representations of individual many-body interactions that are machine-learned from CCSD(T) reference data. Due to its construction, MB-pol is fully transferable across all phases and has been shown to accurately reproduce the properties of gas-phase water clusters, liquid water, and ice.^{69–74} Notably, MB-pol is the first and, to date, only model capable of accurately predicting the phase diagram of water.⁷⁵ More recently, an updated version of MB-pol, MB-pol(2023), trained on larger training sets of CCSD(T) many-body energies, has been shown to achieve even higher predictive accuracy for simulations of water in both gas and liquid phases.⁷⁶ When combined with ab initio-based FFs specifically designed to describe the physicochemical properties of MOFs, MB-pol has enabled realistic molecular dynamics (MD) simulations of water adsorption in several MOFs, providing molecular-level insights into the underlying adsorption mechanisms that are difficult to access experimentally.^{77–82}

In this study, we investigate the adsorption mechanisms of water in MOF-808,²¹ a MOF sharing the same Zr-oxo cluster as UiO-66.⁸³ Despite this similarity, MOF-808 and UiO-66 exhibit differences in their organic linker and connectivity topology, resulting in materials with distinct pore sizes and shapes. The SBU of MOF-808 corresponds to a 6-connected

Zr-oxo cluster that leads to a framework with large adamantane-shaped pores (18.4 Å in diameter) juxtaposed with small tetrahedral pores (4.8 Å in diameter). Conversely, the SBU of UiO-66 corresponds to a 12-connected Zr-oxo cluster, resulting in a framework with octahedral pores (7.2 Å in diameter) encircled by small tetrahedral pores (6.8 Å in diameter). These structural differences not only underline distinct structural properties of the corresponding frameworks but also affect the potential of MOF-808 and UiO-66 in AWH applications. Leveraging MD simulations performed with the MB-pol potential, we elucidate the adsorption mechanism of water within MOF-808 and compare it to the mechanism reported for UiO-66 in Ref. 81. These comparisons allow us to assess how differences in connectivity and bonding topologies between MOF-808 and UiO-66 influence water adsorption in these two MOFs, providing fundamental insights for the design of MOFs specifically optimized for AWH applications.

II. METHODS

A. Force field

The structure of MOF-808, taken from crystallographic data,²¹ was initially optimized in periodic boundary conditions using density functional theory (DFT) calculations carried out with the Vienna Ab initio Simulation Package (VASP).⁸⁴⁻⁸⁷ The VASP calculations were carried out with the PBE exchange-correlation functional⁸⁸ combined with the D3 dispersion correction,⁸⁹ using the projector-augmented wave (PAW)^{90,91} method with a 400 eV kinetic energy cutoff on a $1 \times 1 \times 1$ k-point grid. The forces were converged to a tolerance of 0.04 eV/Å.

The atomic point charges for the force field were obtained using the Charge Model 5 (CM5)⁹² as implemented in Gaussian 16⁹³ by performing DFT calculations on a cluster model of MOF-808 (see Figure S1 of the Supplementary Material) using the ω B97X-D functional⁹⁴ in combination with the def2-TZVP basis set.⁹⁵ MOF-808 was modeled using a flexible force field. The force field parameters for the bonded terms involving the Zr⁴⁺ atoms were fitted using the genetic algorithm⁹⁶ to ω B97X-D/def2-TZVP single point energies calculated with Gaussian 16⁹³ for 300 distorted configurations of the same cluster model of MOF-808 used in the CM5 calculations. The Lennard-Jones (LJ) parameters for the Zr⁴⁺ atoms were taken

from the Universal Force Field (UFF).³⁶ The force field parameters for the bonded and LJ terms involving the linker atoms were taken from the General Amber Force Field (GAFF).³⁷

Water was represented using the MB-pol potential,^{66–68} a flexible, data-driven many-body model that has been shown to predict the properties of water across various phases with unprecedented accuracy.^{74,75,97–99} Additionally, MB-pol has been successfully used to characterize the behavior of water within various MOFs.^{77–80,82} The Supporting Material includes a brief overview of the main results obtained so far using MB-pol, which aims to provide the reader with an up-to-date perspective on the performance of MB-pol in the context of state-of-the-art computer simulations of water. Water–framework interactions were represented by electrostatic and van der Waals terms. The electrostatic term of MB-pol includes both permanent and induced (i.e., polarization) contributions, which implies that in the MD simulations each MB-pol water molecule could be polarized by other MB-pol water molecules as well as the framework, while the framework was not polarizable. LJ parameters of water were taken from the TIP4P/2005 water model,¹⁰⁰ which was shown to be the closest point-charge model to the MB-pol potential of H₂O.¹⁰¹ Lorentz-Berthelot mixing rules were applied to calculate the LJ parameters describing the interactions between dissimilar atoms. All force field parameters are listed in Tables S1-S4 of the Supplementary Material.

B. Molecular dynamics simulations

All MD simulations, except for the umbrella sampling simulations were performed using an in-house code based on the DL_POLY_2 package¹⁰², which was modified to include MB-pol water.^{66–68} The system consisted of $1 \times 1 \times 1$ primitive cells ($35.076 \text{ \AA} \times 35.076 \text{ \AA} \times 35.076 \text{ \AA}$) in periodic boundary conditions.

Various structural, thermodynamic, and dynamical properties were calculated by carrying out MD simulations in the canonical (NVT : constant number of atoms, volume, and temperature), isothermal-isobaric (NPT : constant number of atoms, pressure, and temperature), and microcanonical (NVE : constant number of atoms, volume, and energy) ensembles. In the NVT and NPT simulations, the temperature was maintained at 298.15 K by a Nosé-Hoover chain of four thermostats.¹⁰³ The NPT ensemble was generated according to the algorithm described in Ref. 104. The equations of motion were propagated with

a time step of 0.2 fs according to the velocity-Verlet algorithm. All nonbonded interactions (i.e., electrostatic and van der Waals interactions) were truncated at an atom-atom distance of 9.0 Å. The long-range electrostatic interactions were treated using the Ewald method.¹⁰⁵

For each RH value considered in this study (ranging from 5% to 90%), the initial positions of the water molecules were generated using Packmol,^{106,107} enforcing a uniform distribution across all MOF-808 void spaces. For each system, the positions of the water molecules were subsequently randomized. This was achieved by conducting a series of three short MD simulations in the *NPT* ensemble at 1000 K (10 ps), 500 K (20 ps), and 300 K (20 ps). Lattice parameters, equilibrium bond distances, and enthalpy of adsorption were then calculated from 1 ns-long *NPT* simulations performed at 1 atm and 298.15 K.

The enthalpy of adsorption at a given RH was calculated as:

$$\Delta H_{\text{ads}} = \frac{U(\text{MOF} + N \cdot \text{H}_2\text{O}) - U(\text{MOF}) - N \times U(\text{H}_2\text{O}) - N \times RT}{N} \quad (1)$$

where N is the number of water molecules, R is the ideal gas law constant, T is the temperature, and $U(\text{MOF} + N \cdot \text{H}_2\text{O})$, $U(\text{MOF})$, and $U(\text{H}_2\text{O})$ are the internal energies water-loaded MOF-808, empty MOF-808, and water, respectively. The dynamical properties and entropy of water were calculated by performing 10 independent 50 ps-long *NVE* simulations with the volume held fixed at the average volume calculated from the *NPT* simulations. The entropy was calculated using the two-phase thermodynamic (2PT) model.¹⁰⁸ All results for UiO-66 were taken from Ref. 81.

To characterize the free energy landscape for water adsorption in MOF-808, we calculated the potential of mean force (PMF) associated with moving a single water molecule along a straight path connecting the centers of mass of the large adamantane pore and the small tetrahedral pore. The PMF was calculated using umbrella sampling simulations were carried out with the Large-scale Atomic/Molecular Massively Parallel Simulator (LAMMPS)¹⁰⁹ package interfaced with the MBX C++¹¹⁰ and PLUMED libraries.^{111,112}

III. RESULTS

A. Thermodynamic Properties

To compare the thermodynamic properties of water adsorbed in the pores of MOF-808 and UiO-66, ΔH_{ads} (Figure 1b) and S_{wat} (Figure 1c) were calculated for both MOFs

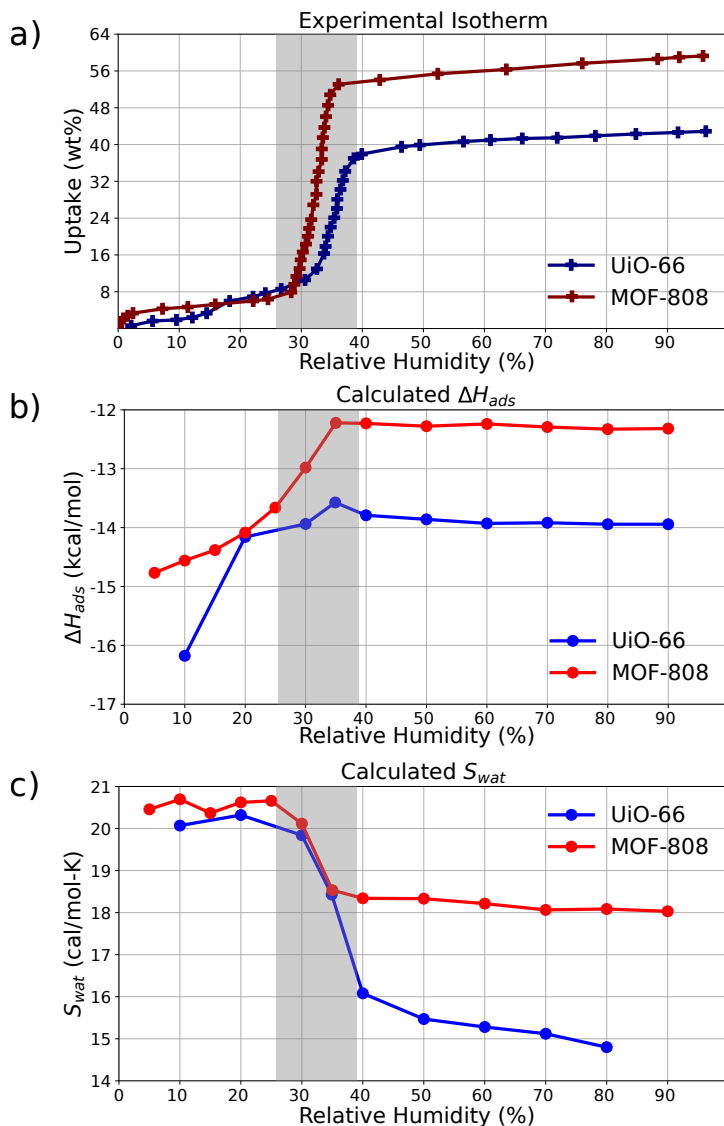


FIG. 1. Thermodynamics of water adsorption in MOF-808 (red) and UiO-66 (blue). a) Experimental adsorption isotherms, b) calculated enthalpies of adsorption (ΔH_{ads}), and c) calculated entropies of water (S_{wat}) as a function of RH. The inflection regions for both MOFs are highlighted in the shaded gray region.

through MD simulations across a range of RH values pertinent to the experimental adsorption isotherms (Figure 1a).²¹

Figure 1b shows that ΔH_{ads} of MOF-808 is most negative (approximately -15.0 kcal/mol-K) at the lowest RH values, indicating relatively stronger water-framework than water-water interactions. Between 25% and 35% RH, there is a notable change in ΔH_{ads} , going from

−13.6 kcal/mol to −12.2 kcal/mol, which correlates well with the inflection point seen in the experimental isotherm (Figure 1a). The decrease of $|\Delta H_{\text{ads}}|$ within this RH range is indicative of less favorable interactions between water molecules and the framework, which also corresponds to an increasing contribution due to hydrogen bonds forming among water molecules. Above 35% RH, ΔH_{ads} reaches a plateau, at approximately −12.3 kcal/mol. This indicates that water–framework interactions become less dominant at higher RH levels. Notably, ΔH_{ads} for water in MOF-808 is more negative than ΔH_{wat} of liquid water at 298 K (approximately −10.96 kcal/mol), as calculated using the MB-pol potential.⁹⁸ This suggests that, on average, the interactions of water molecules within MOF-808 are more favorable than those in bulk liquid water.

In order to disentangle the energy contributions responsible for the variation of ΔH_{ads} at different RH, a decomposition of ΔU_{ads} into water–framework, $U_{\text{wat-MOF}}$, and water–water, $U_{\text{wat-wat}}$, interactions at 5, 30, and 35% RH shown in Figure 2. This analysis indicates that water–framework interactions exhibit maximum strength at low RH and decrease as RH increases and more connected hydrogen-bonding networks form within the MOF pores. In parallel, water–water interactions become the larger contribution beyond the inflection point at 35% RH.

ΔH_{ads} for UiO-66 follows the same trend observed for MOF-808, becoming less negative as RH increases and displaying a notable change between 25% RH and 40% RH in correspon-

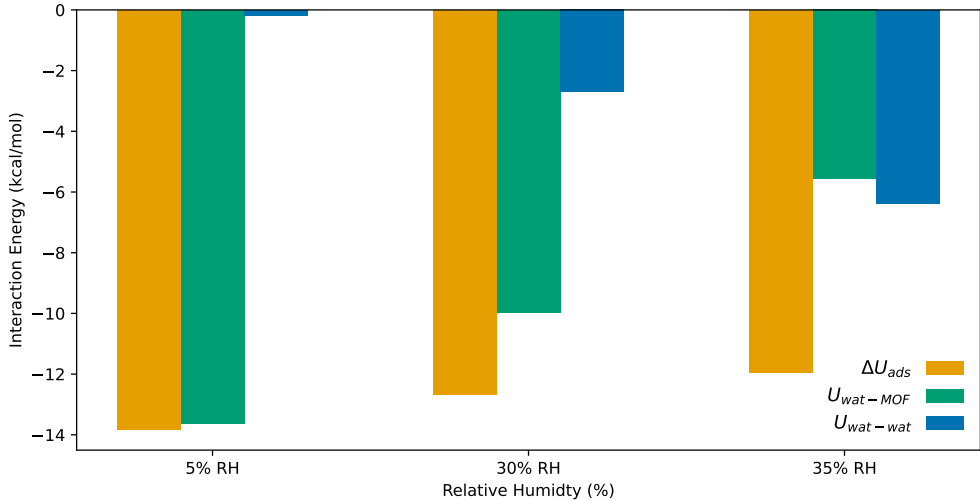


FIG. 2. Decomposition of ΔU_{ads} for MOF-808 at 5, 30, and 35% RH in terms of water–framework, $U_{\text{wat-MOF}}$, and water–water, $U_{\text{wat-wat}}$, energy contributions.

dence with the steep increase in the experimental adsorption isotherm. Beyond 40% RH, ΔH_{ads} levels off for both MOF-808 and UiO-66, consistent with the adsorption isotherms reaching near-maximum pore capacity. Interestingly, at lower RH levels, UiO-66 exhibits a more negative ΔH_{ads} than MOF-808, implying relatively stronger water–framework interactions. At higher RH levels, the more negative value of ΔH_{ads} of UiO-66 compared to MOF-808 suggests that water adsorption into UiO-66 is energetically more favorable than in MOF-808.

The entropy of water, S_{wat} , displays qualitatively similar trends within both MOF-808 and UiO-66. As shown in Figure 1c, at low RH levels, S_{wat} of water in MOF-808 shows minor fluctuations at ~ 20.5 cal/mol-K. With increasing RH, there is a marked decrease in S_{wat} , particularly between 25% and 35% RH, which parallels the significant changes observed in the adsorption enthalpy. This sharp drop in entropy suggests an increase in water confinement within the MOF pores, which is accompanied by the formation of more connected hydrogen-bond networks. S_{wat} within UiO-66 at low RH levels is also approximately 20 cal/mol-K and decreases as RH increases, with the largest drop corresponding to the inflection point of the experimental adsorption isotherm (Figure 1a). Beyond this point, S_{wat} for UiO-66 further decreases to ~ 14.8 cal/mol-K, unlike MOF-808, where S_{wat} remains approximately constant at a value of ~ 18 cal/mol-K. Previous studies of water adsorption in MOFs reported that the average mobility of water molecules within the MOF pores slows down as RH increases and more water molecules participate in hydrogen bonding.^{77,79,82} Given its smaller pore size, UiO-66 thus appears to exert more pronounced confinement effects and pose more constraints on the spatial arrangements of the water molecules. The different trends in S_{wat} indicate that structural differences between MOF-808 and UiO-66 influence the behavior of adsorbed water.

To provide molecular-level insights into the evolution of hydrogen bonding among water molecules within the MOF-808 pores as a function of relative humidity, Figure 3 shows the fraction of different hydrogen-bonding topologies at various RH levels. In this analysis, each water molecule is classified in terms of the number of hydrogen bonds (n or m) it participates in as a donor (D) or an acceptor (A), respectively. At low RH values, the largest fraction (41%) of water molecules does not participate in hydrogen bonding (0D-0A). This value sharply decreases to $\sim 2\%$ by 35% RH in the inflection region. Conversely, a substantial increase in hydrogen bonding occurs after the inflection point, with approximately 98% of

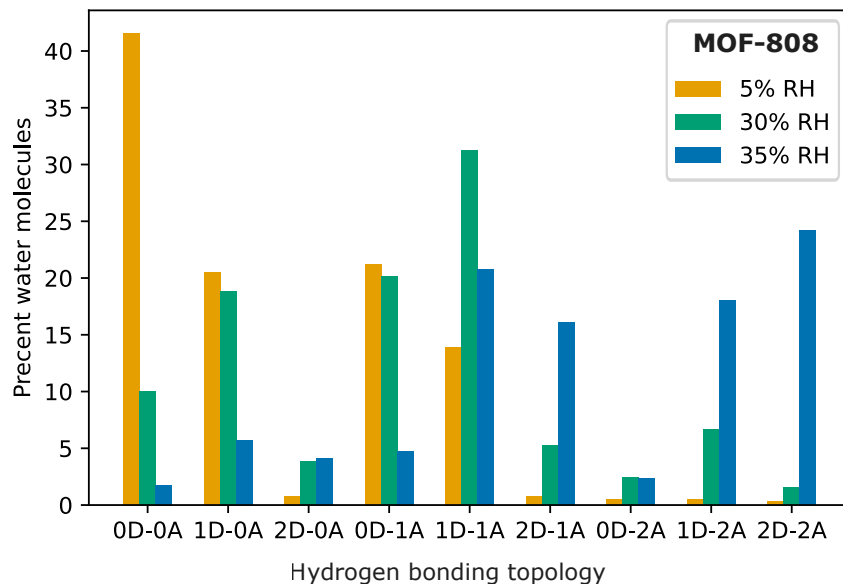


FIG. 3. Probability of different hydrogen-bonding topologies for water within the MOF-808 pores calculated at 5% (yellow), 30% (green), and 35% RH (blue).

water molecules within the MOF-808 pores engaging in hydrogen bonding as indicated by the sum of all fractions of hydrogen-bonding topologies in which a water molecule engages in at least one hydrogen bond. This increase indicates the formation of more connected hydrogen-bonding networks, which modulates the variation of thermodynamic properties as a function of RH as seen in Figure 1.

The comparative analysis of the adsorption enthalpy and water’s entropy in MOF-808 and UiO-66 reveals that the structural differences between these two MOFs play an important role in modulating water adsorption thermodynamics. The 6-connected SBUs of MOF-808 result in larger pores that provide greater freedom to the water molecules, contributing to higher entropy values. In contrast, the 12-connected SBUs of UiO-66 lead to a more compact framework with smaller pores, which is evident in lower entropy values. Interestingly, despite MOF-808 providing larger pores, the plateau of the adsorption enthalpy observed at high RH levels indicates a potential limitation of MOF-808 in fully exploiting the available void space for water adsorption. This observation suggests that pore architecture and connectivity are critical factors in optimizing the performance of MOFs for water harvesting.

B. Spatial arrangement of water within MOF-808 and UiO-66

To gain a deeper understanding of how water interacts with the frameworks of MOF-808 and UiO-66 at low RH levels, Figure 4 shows the radial distribution functions (RDFs) describing the spatial correlations between the oxygen of the water molecules (OW) and the oxygen sites of the framework. As discussed above, MOF-808 and UiO-66 share the same SBUs, which contain three types of oxygen sites: 1) the oxygen atoms of the μ_3 -OH groups, each of which is directly connected to three Zr atoms of the SBU, 2) the hydrogen-uncapped oxygen atoms (μ_3 -O) that are directly connected to three Zr atoms of the SBU, and 3) the oxygen atoms of the carboxylic groups. Due to the 6-connected nature of MOF-808, the oxygen atoms of the carboxylic groups can be further divided into two distinct types, depending on whether they are part of the organic linkers (O_{linker}) or the formate groups (O_{formate}).

The analysis of the RDFs for MOF-808 reveals distinctive peaks at approximately 2.7 Å, 3.1 Å, and 3.5 Å, correlating to the distances between the OW atoms of the water molecules

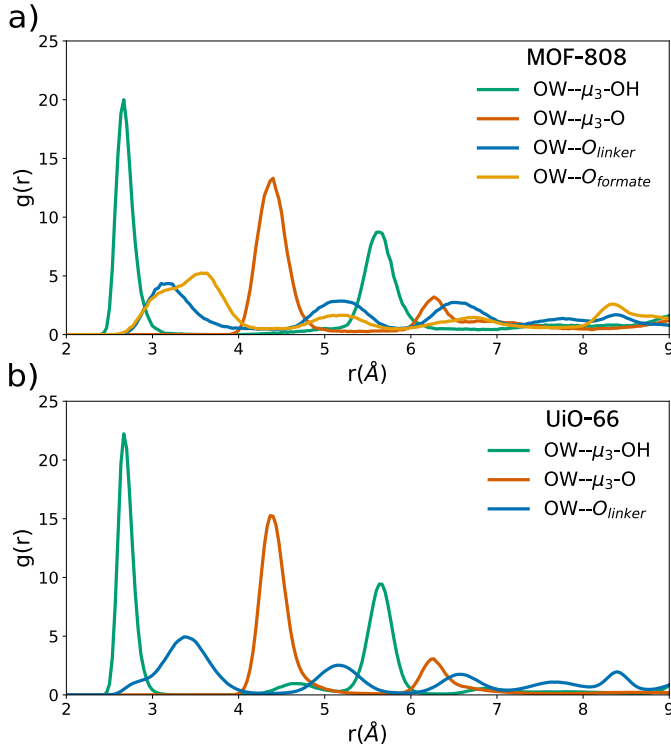


FIG. 4. Radial distribution functions calculated at 10% RH for water in a) MOF-808 and b) UiO-66. See main text for details.

and the μ_3 -OH, O_{linker} , and O_{formate} sites of the framework, respectively. This suggests that the 6-connected SBU of MOF-808 facilitates diverse binding sites for water, with the shortest distance corresponding to the OW and μ_3 -OH interaction. Such an arrangement indicates the formation of relatively strong hydrogen bonds between water and the μ_3 -OH groups of the framework, which is a key step at the early stage of the adsorption process. Similar patterns are found in Figure 4b for the RDFs of water in UiO-66, with the only difference being the location of the main peak of the OW- O_{linker} RDF that appears at a slightly larger distance (3.4 Å) than for water in MOF-808 (3.1 Å). This difference points to the more compact framework of UiO-66, which may restrict the proximity of water molecules to the oxygen atoms of the linkers. Independently of their pore sizes and topologies, both MOF-808 and UiO-66 show a commonality in using their μ_3 -OH groups as primary adsorption sites for water, aligning with other MOFs with similar SBUs. In particular, this trend has been experimentally observed in other MOFs featuring identical SBUs, such as MOF-801.²¹

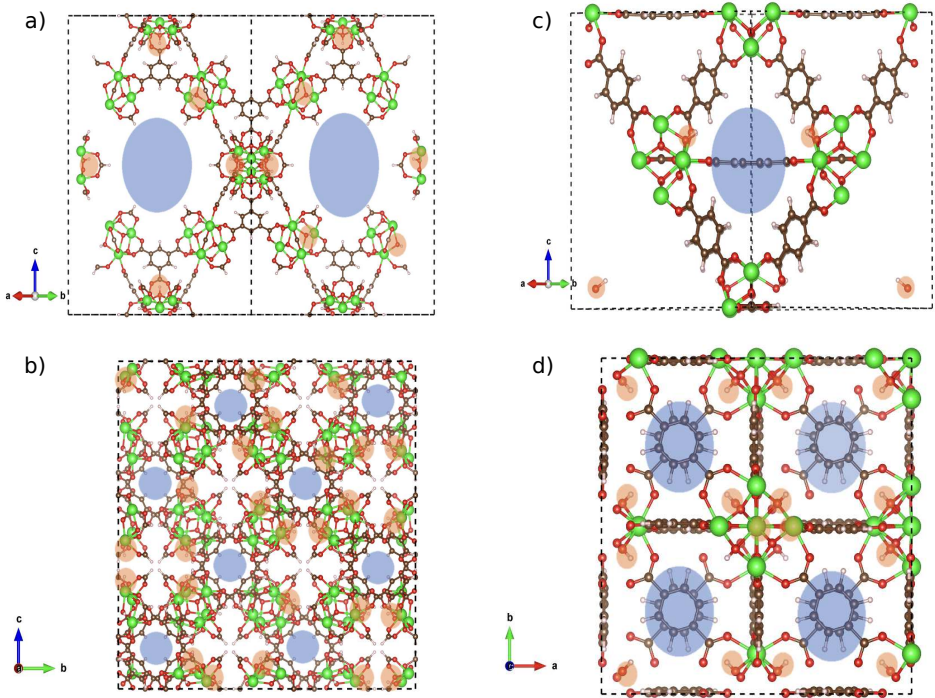


FIG. 5. a-b) View of MOF-808 along the adamantane and tetrahedral pores, respectively. c-d) View of UiO-66 along the octahedral and tetrahedral pores, respectively. The void spaces are shown in blue, while the μ_3 -OH sites are shown in orange. Atom color scheme: C = brown, H = white, O = red, Zr = green.

The distribution of the μ_3 -OH groups in both MOF-808 and UiO-66, illustrated in Figure 5, provides further insights into the spatial arrangement of the water molecules within the pores of the two MOFs at low RH levels. In UiO-66, the μ_3 -OH groups are located within small tetrahedral pores. Conversely, in MOF-808, the μ_3 -OH groups are placed along the large pore perimeters and within small tetrahedral cages, potentially enhancing water adsorption and facilitating efficient pore filling.

C. Pore filling mechanisms

To elucidate the pore-filling mechanism in MOF-808, Figure 6 shows two-dimensional (2D) spatial distributions of water within the small tetrahedral (left) and large adamantane (right) pores calculated at 5% (top), 30% (middle), and 35% RH (bottom). At 5% RH, water molecules in MOF-808 exhibit a strong propensity to form hydrogen bonds with the accessible μ_3 -OH sites on the SBUs, a finding that is in line with the RDF analysis of Section III.B. Notably, the unique distribution of μ_3 -OH sites, predominantly along the periphery of the adamantane pores, impedes the entry of water molecules into the tetrahedral cages at low RH.

To characterize the energetics involved in the diffusion of water molecules from the adamantane to the tetrahedral pores and vice versa, we calculated the potential of mean force (PMF) associated with moving a single water molecule in an empty MOF-808 along a straight path connecting the centers of mass of the adamantane pore and the tetrahedral pore (Figure 7). The PMF shows two minima corresponding to the water molecule being located near the oxygen atoms of the carboxylate group of the linker within the adamantane pore (-3 \AA) and close to the μ_3 -OH group within the tetrahedral pore (3 \AA), respectively. The two minima are separated by a large barrier (greater than 15 kcal/mol from both the adamantane and tetrahedral sides), suggesting an extremely slow diffusion process between the two pores.

This behavior sharply contrasts with that observed in UiO-66, where the analysis of analogous spatial distributions reported in Ref. 81 indicates that water molecules can access the small tetrahedral cages under similar conditions. The difference in water adsorption patterns between MOF-808 and UiO-66 can thus be primarily attributed to the placement of μ_3 -OH groups within their structures. While in UiO-66, these groups effectively facilitate water

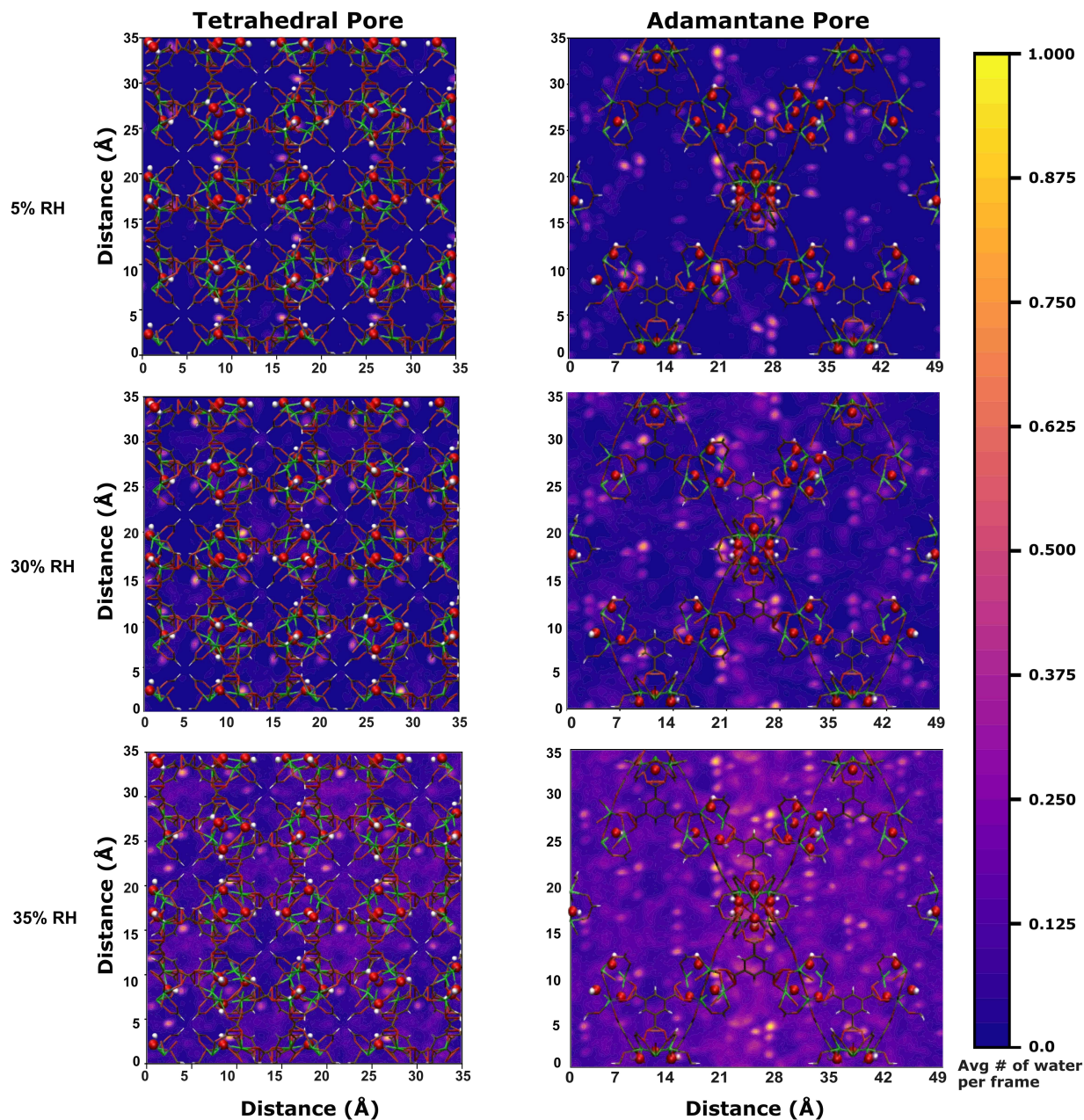


FIG. 6. Two-dimensional water density distribution calculated for tetrahedral pore (left) and adamantane pore (right) at 5% (top), 30% (middle), and 35% RH (bottom). μ_3 -OH sites are illustrated using spheres for significance. The scale bar represents the density of water relative to the highest density region in the unit cell. Atom color scheme: C = brown, H = white, O = red, Zr = green.

entry into the tetrahedral pores, in MOF-808, their arrangement along the pore periphery

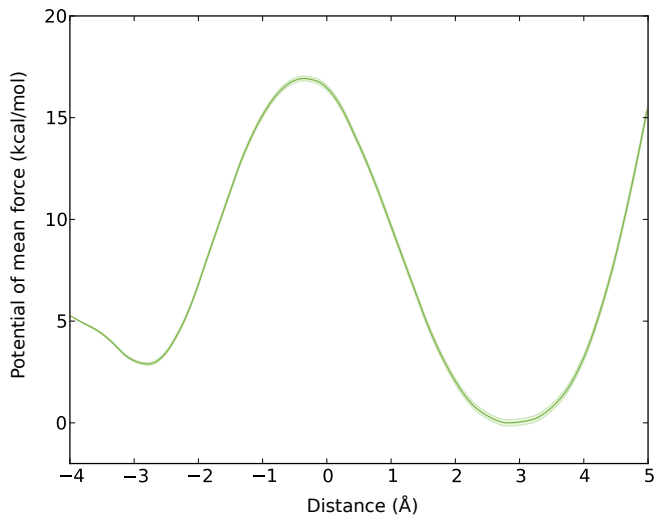


FIG. 7. Potential of mean force (PMF) associated with moving a single water molecule in an empty MOF-808 along a straight path connecting the centers of mass of the adamantane and tetrahedral pores. Negative distances from -4 \AA to 0 \AA correspond to the water molecule being in the adamantane pore and positive distance from 0 \AA to 5 \AA correspond to the water molecule being in the tetrahedral pore, with the channel entrance between the two pores being set to 0 \AA .

creates a barrier that prevents water molecules from entering the small pores, underscoring the critical influence of the μ_3 -OH group distribution in modulating the adsorption mechanism in MOF-808 and UiO-66.

As RH reaches 30%, water molecules not only continue to preferentially bind to the open μ_3 -OH sites but also begin to form more complex structures, like hydrogen-bonded clusters and short chains, with those already bound to the μ_3 -OH sites. This marks a transition from isolated binding to more collective spatial arrangements. At 35% RH, the spatial distributions indicate saturation of both pores in MOF-808, with a preference for filling pores containing water before proceeding to subsequent ones. This behavior has also been seen in analogous MD simulations of water in UiO-66⁸¹, ZIF-90⁷⁸, and ZIF-8.¹¹³ The spatial distribution calculated at 35% RH reveals areas in the adamantane pore that are not completely filled, suggesting that at maximum water capacity, MOF-808 fails to utilize its entire void space for water capture, potentially attributed to the large pore size and the location of the μ_3 -OH sites along the pore perimeters. This finding aligns with previous studies that found that MOFs with larger pore sizes may result in a reduction in water

uptake.¹¹⁴ This phenomenon can be attributed to weakened confinement effects within the pore channels, affecting water–framework and water–water interactions.^{115,116}

The comparison with the simulation results reported in Ref. 81 for UiO-66 indicates that MOF-808 and UiO-66 follow a similar pore-filling mechanism. Despite this similarity, differences in structure and cycle stability between MOF-808 and UiO-66 significantly influence their adsorption capacities.²¹ Experimental data show that, at maximum capacity, MOF-808 adsorbs $\sim 740 \text{ cm}^3 \text{ H}_2\text{O} \cdot \text{g}^{-1} \text{ MOF}$, while UiO-66 adsorbs $\sim 530 \text{ cm}^3 \text{ H}_2\text{O} \cdot \text{g}^{-1} \text{ MOF}$. MOF-808, however, exhibits a decrease in capacity to $\sim 380 \text{ cm}^3 \text{ H}_2\text{O} \cdot \text{g}^{-1} \text{ MOF}$ by the second adsorption cycle, almost a 50% reduction compared to the first cycle. In contrast, UiO-66 maintains a stable capacity of $\sim 500 \text{ cm}^3 \text{ H}_2\text{O} \cdot \text{g}^{-1} \text{ MOF}$. After five cycles, the capacities for MOF-808 and UiO-66 are $\sim 320 \text{ cm}^3 \text{ H}_2\text{O} \cdot \text{g}^{-1} \text{ MOF}$ and $\sim 480 \text{ cm}^3 \text{ H}_2\text{O} \cdot \text{g}^{-1} \text{ MOF}$, respectively. The decrease in adsorption capacity observed for MOF-808 is attributed to the loss of porosity, while the stability of UiO-66 in humid conditions can be explained by the presence of 12-connected SBUs, which allows UiO-66 to maintain consistent water capacity, unaffected by regeneration conditions.²¹ Since both MOF-808 and UiO-66 lack open metal binding sites, the decrease in adsorption capacity observed for MOF-808 has to be related to the connectivity of each SBU to only six linkers. Therefore, while both MOF-808 and UiO-66 share similar adsorption mechanisms, their structural and topological differences clearly affect their cycle stability, underscoring the limitations of MOF-808 in water harvesting. Understanding the degradation of MOFs under humid conditions at the molecular level is a key step towards the design and optimization of MOFs for water harvesting and will be the focus of future applications of our data-driven many-body theoretical/computational platform for modeling aqueous systems under different thermodynamic conditions and in different environments.

IV. CONCLUSIONS

In this study, we employed molecular dynamics simulations to assess the adsorption mechanisms of water in two MOFs, MOF-808 and UiO-66, sharing identical SBUs. Our analysis reveals that both MOF-808 and UiO-66 leverage the μ_3 -OH sites on the SBU for water adsorption. However, the restricted connectivity observed between the SBU and the organic linker in MOF-808 indicates diminished cycle stability performance in comparison

to UiO-66.²¹ Our results underscore the significance of both SBU–organic linker connectivity and the topology of open binding sites in the design of novel MOFs intended for AWH. Building upon insights from pristine MOF-808, we propose further exploration of functionalization strategies to enhance water uptake and cycle stability. Notably, UiO-66 exhibits enhanced water capture capabilities through SBU functionalization, as evidenced in previous studies.^{28,81,117,118} Moreover, MOF-808 demonstrates increased CO₂ uptake upon functionalization compared to its pristine form, as reported in previous investigations.^{119,120} Ongoing research in our group focuses on developing molecular models for various amino acid-functionalized derivatives of MOF-808 to explore ion separation and selectivity from water. In summary, our work contributes a molecular-level understanding of how variations in structure and topology among MOFs with similar architectures influence the overall performance of water harvesting.

V. SUPPLEMENTARY MATERIAL

Details about the molecular models used in the MD simulations along with the complete list of force field parameters used to describe the MOF-808 framework.

VI. ACKNOWLEDGMENTS

This research was supported by the National Science Foundation through award no. 2311260. This research used Expanse at the San Diego Supercomputer Center (SDSC) through allocation CHE230052 from the Advanced Cyberinfrastructure Coordination Ecosystem: Services & Support (ACCESS) program, which is supported by National Science Foundation grants nos. 2138259, 2138286, 2138307, 2137603, and 2138296, as well as the Triton Shared Computing Cluster (TSCC) at SDSC. Kelly M. Hunter, Ching-Hwa Ho, and Jenny Zhang are acknowledged for their guidance and helpful suggestions during this project.

VII. DATA AVAILABILITY

The molecular models used in the MD simulations are publicly available on GitHub(https://github.com/paesanilab/Data_Repository/tree/main/MOF-808) in the format for the

MBX^{110,121} interface with LAMMPS.¹⁰⁹ All computer codes used in the analysis presented in this study are available from the authors upon request.

REFERENCES

- ¹P. Greve, T. Kahil, J. Mochizuki, T. Schinko, Y. Satoh, P. Burek, G. Fischer, S. Tramberend, R. Burtscher, S. Langan, and Y. Wada, “Global assessment of water challenges under uncertainty in water scarcity projections,” *Nat. Sustain.* **1**, 486–494 (2018).
- ²C. He, Z. Liu, J. Wu, X. Pan, Z. Fang, J. Li, and B. A. Bryan, “Future global urban water scarcity and potential solutions,” *Nat. Commun.* **12**, 4667 (2021).
- ³F. Dolan, J. Lamontagne, R. Link, M. Hejazi, P. Reed, and J. Edmonds, “Evaluating the economic impact of water scarcity in a changing world,” *Nat. Commun.* **12**, 1915 (2021).
- ⁴D. Bensen, “How does population growth affect water scarcity?” *Healing Waters International* (2022).
- ⁵United Nations, “Water and climate change,” <https://www.unwater.org/water-facts/water-and-climate-change> (2021).
- ⁶United Nations, “UN Water for Life Decade 2005-2015,” <https://www.un.org/waterforlifedecade/index.shtml>.
- ⁷Centers for Disease Control and Prevention, “Water treatment,” https://www.cdc.gov/healthywater/drinking/public/water_treatment.html.
- ⁸D. W. Hendricks, *Water Treatment Unit Processes: Physical and Chemical*, Vol. 20 (CRC press, 2018).
- ⁹J. Lord, A. Thomas, N. Treat, M. Forkin, R. Bain, P. Dulac, C. H. Behroozi, T. Mamutov, J. Fongheiser, N. Kobilansky, S. Washburn, C. Truesdell, C. Lee, and P. H. Schmaelzle, “Global potential for harvesting drinking water from air using solar energy,” *Nature* **598**, 611–617 (2021).
- ¹⁰Y. Tu, R. Wang, Y. Zhang, and J. Wang, “Progress and expectation of atmospheric water harvesting,” *Joule* **2**, 1452–1475 (2018).
- ¹¹M. Elimelech and W. A. Phillip, “The future of seawater desalination: energy, technology, and the environment,” *Science* **333**, 712–717 (2011).
- ¹²M. A. Shannon, P. W. Bohn, M. Elimelech, J. G. Georgiadis, B. J. Marinas, and A. M. Mayes, “Science and technology for water purification in the coming decades,” *Nature*

- 452**, 301–310 (2008).
- ¹³H. Kim, S. Yang, S. R. Rao, S. Narayanan, E. A. Kapustin, H. Furukawa, A. S. Umans, O. M. Yaghi, and E. N. Wang, “Water harvesting from air with metal-organic frameworks powered by natural sunlight,” *Science* **356**, 430–434 (2017).
- ¹⁴K. Yang, T. Pan, Q. Lei, X. Dong, Q. Cheng, and Y. Han, “A roadmap to sorption-based atmospheric water harvesting: from molecular sorption mechanism to sorbent design and system optimization,” *Environ. Sci. Technol.* **55**, 6542–6560 (2021).
- ¹⁵H. Li, M. Eddaoudi, M. O’Keeffe, and O. M. Yaghi, “Design and synthesis of an exceptionally stable and highly porous metal-organic framework,” *Nature* **402**, 276–279 (1999).
- ¹⁶S. S.-Y. Chui, S. M.-F. Lo, J. P. Charmant, A. G. Orpen, and I. D. Williams, “A chemically functionalizable nanoporous material [Cu₃ (TMA)₂ (H₂O)₃]_n,” *Science* **283**, 1148–1150 (1999).
- ¹⁷D. J. Tranchemontagne, J. L. Mendoza-Cortés, M. O’keeffe, and O. M. Yaghi, “Secondary building units, nets and bonding in the chemistry of metal–organic frameworks,” *Chem. Soc. Rev.* **38**, 1257–1283 (2009).
- ¹⁸J. R. Long and O. M. Yaghi, “The pervasive chemistry of metal–organic frameworks,” *Chem. Soc. Rev.* **38**, 1213–1214 (2009).
- ¹⁹L. Grajciar, O. Bludsky, and P. Nachtigall, “Water adsorption on coordinatively unsaturated sites in Cu-BTC MOF,” *J. Phys. Chem. Lett.* **1**, 3354–3359 (2010).
- ²⁰J. B. DeCoste, G. W. Peterson, B. J. Schindler, K. L. Killops, M. A. Browe, and J. J. Mahle, “The effect of water adsorption on the structure of the carboxylate containing metal–organic frameworks Cu-BTC, Mg-MOF-74, and UiO-66,” *J. Mater. Chem. A* **1**, 11922–11932 (2013).
- ²¹H. Furukawa, F. Gándara, Y.-B. Zhang, J. Jiang, W. L. Queen, M. R. Hudson, and O. M. Yaghi, “Water adsorption in porous metal–organic frameworks and related materials,” *J. Am. Chem. Soc.* **136**, 4369–4381 (2014).
- ²²N. C. Burtch, H. Jasuja, and K. S. Walton, “Water stability and adsorption in metal–organic frameworks,” *Chem. Rev.* **114**, 10575–10612 (2014).
- ²³M. J. Kalmutzki, C. S. Diercks, and O. M. Yaghi, “Metal–organic frameworks for water harvesting from air,” *Adv. Mater.* **30**, 1704304 (2018).
- ²⁴X. Zhang, B. Wang, A. Alsalme, S. Xiang, Z. Zhang, and B. Chen, “Design and applications of water-stable metal-organic frameworks: status and challenges,” *Corrd. Chem.*

- Rev. **423**, 213507 (2020).
- ²⁵P. Küsgens, M. Rose, I. Senkovska, H. Fröde, A. Henschel, S. Siegle, and S. Kaskel, “Characterization of metal-organic frameworks by water adsorption,” *Microporous Mesoporous Mater.* **120**, 325–330 (2009).
- ²⁶P. Ghosh, Y. J. Colón, and R. Q. Snurr, “Water adsorption in UiO-66: the importance of defects,” *ChemComm* **50**, 11329–11331 (2014).
- ²⁷J. Canivet, J. Bonnefoy, C. Daniel, A. Legrand, B. Coasne, and D. Farrusseng, “Structure–property relationships of water adsorption in metal–organic frameworks,” *New J. Chem.* **38**, 3102–3111 (2014).
- ²⁸P. M. Schoenecker, C. G. Carson, H. Jasuja, C. J. Flemming, and K. S. Walton, “Effect of water adsorption on retention of structure and surface area of metal–organic frameworks,” *Ind. Eng. Chem. Res* **51**, 6513–6519 (2012).
- ²⁹J. Canivet, A. Fateeva, Y. Guo, B. Coasne, and D. Farrusseng, “Water adsorption in MOFs: fundamentals and applications,” *Chem. Soc. Rev.* **43**, 5594–5617 (2014).
- ³⁰X. Zhou, H. Lu, F. Zhao, and G. Yu, “Atmospheric water harvesting: a review of material and structural designs,” *ACS Mater. Lett.* **2**, 671–684 (2020).
- ³¹P. G. Mileo, K. H. Cho, J.-S. Chang, and G. Maurin, “Water adsorption fingerprinting of structural defects/capping functions in Zr–fumarate MOFs: a hybrid computational-experimental approach,” *Dalton Trans* **50**, 1324–1333 (2021).
- ³²A. Datar, M. Witman, and L.-C. Lin, “Improving computational assessment of porous materials for water adsorption applications via flat histogram methods,” *J. Phys. Chem. C* **125**, 4253–4266 (2021).
- ³³J. D. Howe, C. R. Morelock, Y. Jiao, K. W. Chapman, K. S. Walton, and D. S. Sholl, “Understanding structure, metal distribution, and water adsorption in mixed-metal MOF-74,” *J. Phys. Chem. C* **121**, 627–635 (2017).
- ³⁴F.-X. Coudert and A. H. Fuchs, “Computational characterization and prediction of metal–organic framework properties,” *Corrd. Chem. Rev.* **307**, 211–236 (2016).
- ³⁵S. L. Mayo, B. D. Olafson, and W. A. Goddard, “DREIDING: a generic force field for molecular simulations,” *J. Phys. Chem.* **94**, 8897–8909 (1990).
- ³⁶A. K. Rappé, C. J. Casewit, K. Colwell, W. A. Goddard III, and W. M. Skiff, “UFF, a full periodic table force field for molecular mechanics and molecular dynamics simulations,” *J. Am. Chem. Soc.* **114**, 10024–10035 (1992).

- ³⁷J. Wang, R. M. Wolf, J. W. Caldwell, P. A. Kollman, and D. A. Case, “Development and testing of a general amber force field,” *J. Comput. Chem.* **25**, 1157–1174 (2004).
- ³⁸K. Vanommeslaeghe, E. Hatcher, C. Acharya, S. Kundu, S. Zhong, J. Shim, E. Darian, O. Guvench, P. Lopes, I. Vorobyov, and A. D. Mackerell Jr., “CHARMM general force field: A force field for drug-like molecules compatible with the CHARMM all-atom additive biological force fields,” *J. Comput. Chem.* **31**, 671–690 (2010).
- ³⁹K. Vanommeslaeghe and A. MacKerell Jr, “CHARMM additive and polarizable force fields for biophysics and computer-aided drug design,” *Biochim. Biophys. Acta* **1850**, 861–871 (2015).
- ⁴⁰J. W. Ponder, C. Wu, P. Ren, V. S. Pande, J. D. Chodera, M. J. Schnieders, I. Haque, D. L. Mobley, D. S. Lambrecht, R. A. DiStasio Jr, M. Head-Gordon, G. N. I. Clark, M. E. Johnson, and T. Head-Gordon, “Current status of the AMOEBA polarizable force field,” *J. Phys. Chem. B* **114**, 2549–2564 (2010).
- ⁴¹G. A. Cisneros, K. T. Wikfeldt, L. Ojamäe, J. Lu, Y. Xu, H. Torabifard, A. P. Bartók, G. Csányi, V. Molinero, and F. Paesani, “Modeling molecular interactions in water: From pairwise to many-body potential energy functions,” *Chem. Rev.* **116**, 7501–7528 (2016).
- ⁴²Z. Jing, C. Liu, S. Y. Cheng, R. Qi, B. D. Walker, J.-P. Piquemal, and P. Ren, “Polarizable force fields for biomolecular simulations: Recent advances and applications,” *Annu. Rev. Biophys.* **48**, 371–394 (2019).
- ⁴³V. S. Inakollu, D. P. Geerke, C. N. Rowley, and H. Yu, “Polarisable force fields: what do they add in biomolecular simulations?” *Curr. Opin. Struct. Biol.* **61**, 182–190 (2020).
- ⁴⁴A. Szabo and N. S. Ostlund, *Modern Quantum Chemistry*. (Dover, 1996).
- ⁴⁵R. Parr, *Density Functional Theory of Atoms and Molecules. In Horizons of Quantum Chemistry (pp.5–15)* (Springer, 1980).
- ⁴⁶J. F. Stanton, “Why CCSD(T) works: A different perspective,” *Chem. Phys. Lett.* **281**, 130–134 (1997).
- ⁴⁷J. Rezac and P. Hobza, “Benchmark calculations of interaction energies in noncovalent complexes and their applications,” *Chem. Rev.* **116**, 5038–5071 (2016).
- ⁴⁸J. Zang, S. Nair, and D. S. Sholl, “Prediction of water adsorption in copper-based metal-organic frameworks using force fields derived from dispersion-corrected DFT calculations,” *J. Phys. Chem. C* **117**, 7519–7525 (2013).

- ⁴⁹X. Peng, L.-C. Lin, W. Sun, and B. Smit, “Water adsorption in metal–organic frameworks with open-metal sites,” *AIChE J* **61**, 677–687 (2015).
- ⁵⁰Y. Ming, N. Kumar, and D. J. Siegel, “Water adsorption and insertion in MOF-5,” *ACS Omega* **2**, 4921–4928 (2017).
- ⁵¹J. P. Perdew and A. Zunger, “Self-interaction correction to density-functional approximations for many-electron systems,” *Phys. Rev. B* **23**, 5048 (1981).
- ⁵²P. Mori-Sánchez, A. J. Cohen, and W. Yang, “Localization and delocalization errors in density functional theory and implications for band-gap prediction,” *Phys. Rev. Lett.* **100**, 146401 (2008).
- ⁵³M.-C. Kim, E. Sim, and K. Burke, “Understanding and reducing errors in density functional calculations,” *Phys. Rev. Lett.* **111**, 073003 (2013).
- ⁵⁴M.-C. Kim, E. Sim, and K. Burke, “Ions in solution: Density corrected density functional theory (DC-DFT),” *J. Chem. Phys.* **140**, 18A528 (2014).
- ⁵⁵M.-C. Kim, H. Park, S. Son, E. Sim, and K. Burke, “Improved DFT potential energy surfaces via improved densities,” *J. Phys. Chem. Lett.* **6**, 3802–3807 (2015).
- ⁵⁶E. Sim, S. Song, and K. Burke, “Quantifying density errors in DFT,” *J. Phys. Chem. Lett.* **9**, 6385–6392 (2018).
- ⁵⁷E. Sim, S. Song, S. Vuckovic, and K. Burke, “Improving results by improving densities: Density-corrected density functional theory,” *J. Am. Chem. Soc.* **144**, 6625–6639 (2022).
- ⁵⁸S. Dasgupta, E. Lambros, J. P. Perdew, and F. Paesani, “Elevating density functional theory to chemical accuracy for water simulations through a density-corrected many-body formalism,” *Nuovo Cimento* **12**, 6359 (2021).
- ⁵⁹E. Palos, E. Lambros, S. Swee, J. Hu, S. Dasgupta, and F. Paesani, “Assessing the interplay between functional-driven and density-driven errors in DFT models of water,” *J. Chem. Theory Comput.* **18**, 3410–3426 (2022).
- ⁶⁰S. Dasgupta, C. Shahi, P. Bhetwal, J. P. Perdew, and F. Paesani, “How good is the density-corrected SCAN functional for neutral and ionic aqueous systems, and what is so right about the Hartree–Fock density?” *J. Chem. Theory Comput.* **18**, 4745–4761 (2022).
- ⁶¹E. Palos, S. Dasgupta, E. Lambros, and F. Paesani, “Data-driven many-body potentials from density functional theory for aqueous phase chemistry,” *Chem. Phys. Rev.* **4** (2023).
- ⁶²E. Palos, A. Caruso, and F. Paesani, “Consistent density functional theory-based description of ion hydration through density-corrected many-body representations,” *The Journal*

- of Chemical Physics **159** (2023).
- ⁶³C. Vega and J. L. Abascal, “Simulating water with rigid non-polarizable models: a general perspective,” *Phys. Chem. Chem. Phys.* **13**, 19663–19688 (2011).
- ⁶⁴R. Sakamaki, A. K. Sum, T. Narumi, and K. Yasuoka, “Molecular dynamics simulations of vapor/liquid coexistence using the nonpolarizable water models,” *J. Chem. Phys.* **134**, 124708 (2011).
- ⁶⁵C. Vega, J. Abascal, and I. Nezbeda, “Vapor-liquid equilibria from the triple point up to the critical point for the new generation of TIP4P-like models: TIP4P/Ew, TIP4P/2005, and TIP4P/ice,” *J. Chem. Phys.* **125**, 34503 (2006).
- ⁶⁶V. Babin, C. Leforestier, and F. Paesani, “Development of a “first principles” water potential with flexible monomers: Dimer potential energy surface, VRT spectrum, and second virial coefficient,” *J. Chem. Theory Comput.* **9**, 5395–5403 (2013).
- ⁶⁷V. Babin, G. R. Medders, and F. Paesani, “Development of a “first principles” water potential with flexible monomers. II: Trimer potential energy surface, third virial coefficient, and small clusters,” *J. Chem. Theory Comput.* **10**, 1599–1607 (2014).
- ⁶⁸G. R. Medders, V. Babin, and F. Paesani, “Development of a “first-principles” water potential with flexible monomers. III. liquid phase properties,” *J. Chem. Theory Comput.* **10**, 2906–2910 (2014).
- ⁶⁹S. E. Brown, A. W. Götz, X. Cheng, R. P. Steele, V. A. Mandelshtam, and F. Paesani, “Monitoring water clusters “melt” through vibrational spectroscopy,” *J. Am. Chem. Soc.* **139**, 7082–7088 (2017).
- ⁷⁰J. O. Richardson, C. Pérez, S. Lobsiger, A. A. Reid, B. Temelso, G. C. Shields, Z. Kisiel, D. J. Wales, B. H. Pate, and S. C. Althorpe, “Concerted hydrogen-bond breaking by quantum tunneling in the water hexamer prism,” *Science* **351**, 1310–1313 (2016).
- ⁷¹W. T. Cole, J. D. Farrell, D. J. Wales, and R. J. Saykally, “Structure and torsional dynamics of the water octamer from THz laser spectroscopy near 215 μm ,” *Science* **352**, 1194–1197 (2016).
- ⁷²G. R. Medders and F. Paesani, “Infrared and raman spectroscopy of liquid water through “first-principles” many-body molecular dynamics,” *J. Chem. Theory Comput.* **11**, 1145–1154 (2015).
- ⁷³D. R. Moberg, S. C. Straight, and F. Paesani, “Temperature dependence of the air/water interface revealed by polarization sensitive sum-frequency generation spectroscopy,” *J.*

- Phys. Chem. B. **122**, 4356–4365 (2018).
- ⁷⁴M. C. Muniz, T. E. Gartner, M. Riera, C. Knight, S. Yue, F. Paesani, and A. Z. Panagiotopoulos, “Vapor–liquid equilibrium of water with the MB-pol many-body potential,” J. Chem. Phys. **154** (2021).
- ⁷⁵S. L. Bore and F. Paesani, “Realistic phase diagram of water from “first principles” data-driven quantum simulations,” Nat. Commun. **14**, 3349 (2023).
- ⁷⁶X. Zhu, M. Riera, E. F. Bull-Vulpe, and F. Paesani, “MB-pol (2023): Sub-chemical accuracy for water simulations from the gas to the liquid phase,” J. Chem. Theory Comput. (2023).
- ⁷⁷A. J. Rieth, K. M. Hunter, M. Dincă, and F. Paesani, “Hydrogen bonding structure of confined water templated by a metal-organic framework with open metal sites,” Nat. Commun. **10**, 4771 (2019).
- ⁷⁸J. C. Wagner, K. M. Hunter, F. Paesani, and W. Xiong, “Water capture mechanisms at zeolitic imidazolate framework interfaces,” J. Am. Chem. Soc. **143**, 21189–21194 (2021).
- ⁷⁹K. M. Hunter, J. C. Wagner, M. Kalaj, S. M. Cohen, W. Xiong, and F. Paesani, “Simulation meets experiment: unraveling the properties of water in metal–organic frameworks through vibrational spectroscopy,” J. Phys. Chem. C **125**, 12451–12460 (2021).
- ⁸⁰C.-H. Ho, M. L. Valentine, Z. Chen, H. Xie, O. Farha, W. Xiong, and F. Paesani, “Structure and thermodynamics of water adsorption in NU-1500-Cr,” Commun. Chem. **6**, 70 (2023).
- ⁸¹J. Zhang, F. Paesani, and M. Lessio, “Computational insights into the interaction of water with the UiO-66 metal-organic framework and its functionalized derivatives,” J. Mater. Chem. C **11**, 10247–10258 (2023).
- ⁸²C.-H. Ho and F. Paesani, “Elucidating the competitive adsorption of H₂O and CO₂ in CALF-20: new insights for enhanced carbon capture metal–organic frameworks,” ACS Appl. Mater. Interfaces. **15**, 48287–48295 (2023).
- ⁸³J. H. Cavka, S. Jakobsen, U. Olsbye, N. Guillou, C. Lamberti, S. Bordiga, and K. P. Lillerud, “A new zirconium inorganic building brick forming metal organic frameworks with exceptional stability,” J. Am. Chem. Soc. **130**, 13850–13851 (2008).
- ⁸⁴G. Kresse and J. Hafner, “Ab initio molecular dynamics for liquid metals,” Phys. Rev. B **47**, 558 (1993).

- ⁸⁵G. Kresse and J. Hafner, “Ab initio molecular-dynamics simulation of the liquid-metal–amorphous-semiconductor transition in germanium,” *Phys. Rev. B* **49**, 14251 (1994).
- ⁸⁶G. Kresse and J. Furthmüller, “Efficiency of ab-initio total energy calculations for metals and semiconductors using a plane-wave basis set,” *Comput. Mater. Sci.* **6**, 15–50 (1996).
- ⁸⁷G. Kresse and J. Furthmüller, “Efficient iterative schemes for ab initio total-energy calculations using a plane-wave basis set,” *Phys. Rev. B* **54**, 11169 (1996).
- ⁸⁸J. P. Perdew, K. Burke, and M. Ernzerhof, “Generalized gradient approximation made simple,” *Phys. Rev. Lett.* **77**, 3865 (1996).
- ⁸⁹S. Grimme, J. Antony, S. Ehrlich, and H. Krieg, “A consistent and accurate ab initio parametrization of density functional dispersion correction (DFT-D) for the 94 elements H-Pu,” *J. Chem. Phys.* **132**, 154104 (2010).
- ⁹⁰P. E. Blöchl, “Projector augmented-wave method,” *Phys. Rev. B* **50**, 17953 (1994).
- ⁹¹G. Kresse and D. Joubert, “From ultrasoft pseudopotentials to the projector augmented-wave method,” *Phys. Rev. B* **59**, 1758 (1999).
- ⁹²A. V. Marenich, S. V. Jerome, C. J. Cramer, and D. G. Truhlar, “Charge model 5: An extension of hirshfeld population analysis for the accurate description of molecular interactions in gaseous and condensed phases,” *J. Chem. Theory Comput.* **8**, 527–541 (2012).
- ⁹³M. J. Frisch, G. W. Trucks, H. B. Schlegel, G. E. Scuseria, M. A. Robb, J. R. Cheeseman, G. Scalmani, V. Barone, G. A. Petersson, H. Nakatsuji, X. Li, M. Caricato, A. V. Marenich, J. Bloino, B. G. Janesko, R. Gomperts, B. Mennucci, H. P. Hratchian, J. V. Ortiz, A. F. Izmaylov, J. L. Sonnenberg, D. Williams-Young, F. Ding, F. Lipparini, F. Egidi, J. Goings, B. Peng, A. Petrone, T. Henderson, D. Ranasinghe, V. G. Zakrzewski, J. Gao, N. Rega, G. Zheng, W. Liang, M. Hada, M. Ehara, K. Toyota, R. Fukuda, J. Hasegawa, M. Ishida, T. Nakajima, Y. Honda, O. Kitao, H. Nakai, T. Vreven, K. Throssell, J. A. Montgomery, Jr., J. E. Peralta, F. Ogliaro, M. J. Bearpark, J. J. Heyd, E. N. Brothers, K. N. Kudin, V. N. Staroverov, T. A. Keith, R. Kobayashi, J. Normand, K. Raghavachari, A. P. Rendell, J. C. Burant, S. S. Iyengar, J. Tomasi, M. Cossi, J. M. Millam, M. Klene, C. Adamo, R. Cammi, J. W. Ochterski, R. L. Martin, K. Morokuma, O. Farkas, J. B. Foresman, and D. J. Fox, “Gaussian 16 Revision A.03,” (2016), Gaussian Inc. Wallingford CT.

- ⁹⁴J.-D. Chai and M. Head-Gordon, “Long-range corrected hybrid density functionals with damped atom–atom dispersion corrections,” *Phys. Chem. Chem. Phys.* **10**, 6615–6620 (2008).
- ⁹⁵F. Weigend, “Accurate coulomb-fitting basis sets for H to Rn,” *Phys. Chem. Chem. Phys.* **8**, 1057–1065 (2006).
- ⁹⁶“D.L. Carroll’s FORTRAN Genetic Algorithm Driver v1.7a,” <https://cuaerospace.com/products-services/genetic-algorithm> (2001).
- ⁹⁷F. Paesani, “Getting the right answers for the right reasons: Toward predictive molecular simulations of water with many-body potential energy functions,” *Acc. Chem. Res.* **49**, 1844–1851 (2016).
- ⁹⁸S. K. Reddy, S. C. Straight, P. Bajaj, C. H. Pham, M. Riera, D. R. Moberg, M. A. Morales, C. Knight, A. W. Götz, and F. Paesani, “On the accuracy of the MB-pol many-body potential for water: Interaction energies, vibrational frequencies, and classical thermodynamic and dynamical properties from clusters to liquid water and ice,” *J. Chem. Phys.* **145**, 194504 (2016).
- ⁹⁹T. E. Gartner III, K. M. Hunter, E. Lambros, A. Caruso, M. Riera, G. R. Medders, A. Z. Panagiotopoulos, P. G. Debenedetti, and F. Paesani, “Anomalies and local structure of liquid water from boiling to the supercooled regime as predicted by the many-body MB-pol model,” *J. Phys. Chem. Lett.* **13**, 3652–3658 (2022).
- ¹⁰⁰J. L. F. Abascal and C. Vega, “A general purpose model for the condensed phases of water: TIP4P/2005,” *J. Chem. Phys.* **123**, 234505 (2005).
- ¹⁰¹G. R. Medders and F. Paesani, “On the interplay of the potential energy and dipole moment surfaces in controlling the infrared activity of liquid water,” *J. Chem. Phys.* **142** (2015).
- ¹⁰²W. Smith and T. Forester, “DL_POLY_2. 0: A general-purpose parallel molecular dynamics simulation package,” *J. Mol. Graph.* **14**, 136–141 (1996).
- ¹⁰³M. E. Tuckerman, A. Chandra, and D. Marx, “A statistical mechanical theory of proton transport kinetics in hydrogen-bonded networks based on population correlation functions with applications to acids and bases,” *J. Chem. Phys.* **133**, 124108 (2010).
- ¹⁰⁴G. J. Martyna, A. Hughes, and M. E. Tuckerman, “Molecular dynamics algorithms for path integrals at constant pressure,” *J. Chem. Phys.* **110**, 3275–3290 (1999).
- ¹⁰⁵A. R. Leach, *Molecular modelling: principles and applications* (Pearson education, 2001).

- ¹⁰⁶L. Martínez, R. Andrade, E. G. Birgin, and J. M. Martínez, “PACKMOL: a package for building initial configurations for molecular dynamics simulations,” *J. Comput. Chem.* **30**, 2157–2164 (2009).
- ¹⁰⁷J. M. Martínez and L. Martínez, “Packing optimization for automated generation of complex system’s initial configurations for molecular dynamics and docking,” *J. Comput. Chem.* **24**, 819–825 (2003).
- ¹⁰⁸S.-T. Lin, P. K. Maiti, and W. A. Goddard III, “Two-phase thermodynamic model for efficient and accurate absolute entropy of water from molecular dynamics simulations,” *J. Phys. Chem. B* **114**, 8191–8198 (2010).
- ¹⁰⁹A. P. Thompson, H. M. Aktulga, R. Berger, D. S. Bolintineanu, W. M. Brown, P. S. Crozier, P. J. in ’t Veld, A. Kohlmeyer, S. G. Moore, T. D. Nguyen, R. Shan, M. J. Stevens, J. Tranchida, C. Trott, and S. J. Plimpton, “LAMMPS - A flexible simulation tool for particle-based materials modeling at the atomic, meso, and continuum scales,” *Comput. Phys. Commun.* **271**, 108171 (2022).
- ¹¹⁰“MBX v1.0,” <https://paesanigroup.ucsd.edu/software/mbx.html> (2023).
- ¹¹¹M. Bonomi, D. Branduardi, G. Bussi, C. Camilloni, D. Provasi, P. Raiteri, D. Donadio, F. Marinelli, F. Pietrucci, R. A. Broglia, *et al.*, “Plumed: A portable plugin for free-energy calculations with molecular dynamics,” *Computer Physics Communications* **180**, 1961–1972 (2009).
- ¹¹²G. A. Tribello, M. Bonomi, D. Branduardi, C. Camilloni, and G. Bussi, “Plumed 2: New feathers for an old bird,” *Computer physics communications* **185**, 604–613 (2014).
- ¹¹³H. Zhang and R. Q. Snurr, “Computational study of water adsorption in the hydrophobic metal–organic framework ZIF-8: adsorption mechanism and acceleration of the simulations,” *J. Phys. Chem. C* **121**, 24000–24010 (2017).
- ¹¹⁴H. Furukawa, K. E. Cordova, M. O’Keeffe, and O. M. Yaghi, “The chemistry and applications of metal-organic frameworks,” *Science* **341**, 1230444 (2013).
- ¹¹⁵L. Gilmanova, V. Bon, L. Shupletsov, D. Pohl, M. Rauche, E. Brunner, and S. Kaskel, “Chemically stable carbazole-based imine covalent organic frameworks with acidochromic response for humidity control applications,” *J. Am. Chem. Soc.* **143**, 18368–18373 (2021).
- ¹¹⁶X. Liu, X. Wang, and F. Kapteijn, “Water and metal–organic frameworks: from interaction toward utilization,” *Chem. Rev.* **120**, 8303–8377 (2020).

- ¹¹⁷N. Hanikel, M. S. Prévot, and O. M. Yaghi, “MOF water harvesters,” *Nat. Nanotechnol.* **15**, 348–355 (2020).
- ¹¹⁸X. Tang, Y. Luo, Z. Zhang, W. Ding, D. Liu, J. Wang, L. Guo, and M. Wen, “Effects of functional groups of–NH₂ and–NO₂ on water adsorption ability of Zr-based MOFs (UiO-66),” *Chem. Phys.* **543**, 111093 (2021).
- ¹¹⁹H. Lyu, O. I.-F. Chen, N. Hanikel, M. I. Hossain, R. W. Flaig, X. Pei, A. Amin, M. D. Doherty, R. K. Impastato, T. G. Glover, D. R. Moore, and O. M. Yaghi, “Carbon dioxide capture chemistry of amino acid functionalized metal–organic frameworks in humid flue gas,” *J. Am. Chem. Soc.* **144**, 2387–2396 (2022).
- ¹²⁰T. M. Rayder, F. Formalik, S. M. Vornholt, H. Frank, S. Lee, M. Alzayer, Z. Chen, D. Sengupta, T. Islamoglu, F. Paesani, K. W. Chapman, R. Q. Snurr, and O. K. Farha, “Unveiling unexpected modulator-CO₂ dynamics within a Zirconium metal–organic framework,” *J. Am. Chem. Soc.* **145**, 11195–11205 (2023).
- ¹²¹M. Riera, C. Knight, E. F. Bull-Vulpe, X. Zhu, H. Agnew, D. G. A. Smith, A. C. Simonett, and F. Paesani, “MBX: A many-body energy and force calculator for data-driven many-body simulations,” *J. Chem. Phys.* **159**, 054802 (2023).